arXiv:1210.4268v1 [cond-mat.mes-hall] 16 Oct 2012

Electronic ground state properties of strained graphene

H. Rostami[1] and Reza Asgari[1,*]

[1]School of Physics, Institute for Research in Fundamental Sciences (IPM), Tehran 19395-5531, Iran

(Dated: October 17, 2012)

We consider the effect of the Coulomb interaction in strained graphene using tight-binding approximation together with the Hartree-Fock interactions. The many-body energy dispersion relation, anisotropic Fermi velocity renormalization and charge compressibility in the presence of uniaxial strain are calculated. We show that the quasiparticle quantities are sensitive to homogenous strain and indeed, to its sign. The charge compressibility is enhanced by stretching and suppressed by compressing a graphene sheet. We find a reduction of Fermi velocity renormalization along the direction of graphene deformation, in good agreement with the recent experimental observation.

PACS numbers: 71.10.Ca, 68.35.Gy, 71.18.+y

I. INTRODUCTION

Graphene is a two-dimensional crystal of carbon atoms with enormous interest on its unique features[1]. Graphene sheet has attracted considerable attention because of its unusual electronic properties[2,3] which follow from chiral band states and because of potential applications[4]. The low energy quasiparticle excitations energies in graphene are linearly dispersing, described by Dirac cones at the edges of the first Brillouin zone. Charge carriers move strictly in two-dimensions since the graphene layer is just one atomic monolayer thick.

Graphene is amenable to external influences incorporating mechanical deformation[5,6]. Its band structure does not change for realistic strains less than 15%[6,7]. The influence of long-range strains on the electronic properties is a unique feature of graphene[8,9]. At low-energy spectrum, strains give rise to a pseudomagnetic field which is added to the momentum operators[10] and thus a gauge field couples to electrons. The most evidence of the unusual way in which strains affect the electronic states comes from scanning tunneling microscope measurements of the electronic local density of states of graphene grown on platinum[11]. An average compression of 10% creates effective fields of the same order of magnitude with the value observed in experiments[12].

Tuning the dynamics of massless carriers by appropriately designed strain patterns[13] opens the way for novel applications of graphene[14]. Strain can be induced in graphene either intentionally or naturally. Uniaxial strain can be induced by bending the substrates on which graphene is elongated without slippage. Elastic responses have been measured by pushing a tip of atomic force microscopes on suspended graphene. The presence of ripples in graphene samples and their influence on the electronic properties are open problems in the field for instance graphene on top of SiO_2 or SiC surface experiences a moderate strain due to surface corrugations or lattice mismatch.

The Fermi velocity is an essential quantity in graphene because all the observable quantities depend on it. For the Dirac electrons in pristine graphene, it was shown[15–20] that interaction effects also become noticeable with decreasing density in that the velocity is enhanced rather than suppressed, and that the influence of interactions on the compressibility and the spin-susceptibility changes sign. These qualitative differences are due to *exchange interactions* between electrons near the Fermi surface and electrons in the negative energy sea and to interband contributions to Dirac electrons from charge and spin fluctuations. Recent experiments[20,21] have been able to measure the renormalized Fermi velocity and they claimed that the Fermi velocity is no longer constant but increases by decreasing the electron density. On the other hand, it was shown[22], from first principles calculations, that the group velocities under uniaxial strain exhibit a strong anisotropy. As the uniaxial strain increases along a certain direction, the Fermi velocity parallel to it decreases quickly and vanishes eventually, whereas the Fermi velocity perpendicular to it increases by as much as 25%. It was also shown that the work function of strained graphene increases substantially as strain increases.

The role of long-range electron-electron interactions in a uniaxial strain on undoped graphene, has been recently studied[23] using the renormalization group theory. They showed that while for small interactions and anisotropy the system restores the conventional isotropic Dirac liquid behavior, at intermediate coupling both the anisotropy and interactions can flow, in the renormalization group sense, toward large values thus signaling the emergence of anisotropic excitonic states. On the other hand, the dependence of the electron velocity on periodic deformations of graphene has also been investigated by another group[24]. The authors showed that the Fermi velocity anisotropy corresponds to the anisotropy of the quasiparticle spectrum energy.

The positions of the Dirac points can be shifted in the opposite directions by applying anisotropic strains. The reason for this is that the time-reversal symmetry is preserved by strain in graphene[25]. However, the translational symmetry is broken by lattice deformation.

Our aim in this work is to study the Coulomb interaction effects in uniaxially strained graphene particulary the anisotropy of the Fermi velocity renormalization and

the charge compressibility within the exchange interaction. In the Hartree-Fock theory, the positions of the Dirac points are shifted in the opposite directions when the full Brillouin zone calculation is taken into account. Our theory for strain dependence of quasiparticle velocity renormalization in interacting Dirac electron systems is motivated not only by fundamental many-body considerations, but also by application and potential future experiments in the strain engineering field.

The paper is organized as follows. In Sec. II we introduce the formalism that will be used in calculating strained ground state properties which includes the many-body effects by using Hartree-Fock (HF) approximation. In Sec. III we present our analytical and numerical results for the renormalized Fermi velocity and the charge compressibility in doped graphene sheets. Sec. IV contains discussions and conclusions.

II. METHOD AND THEORY

A. Noninteractacting strained graphene

The electronic bands in graphene arise from the hybridization of p_z orbitals which are localized at each carbon atom. A good description of the electron states is obtained by assuming that electrons can hop between nearest-neighbor atoms. We consider a two dimensional honeycomb lattice in which a p_z electron hops between lattice points and it is governed by the nearest-neighbor tight-binding Hamiltonian

$$H_0 = -\sum_{<ij>} t_{ij} a_i^\dagger b_j + H.c\ . \tag{1}$$

where a_i and b_j are fermion field operators in sublattices A and B, t_{ij} are hopping integrals between lattice points and will be different among different neighbors. The Fourier component of the Hamiltonian is written as

$$H_0^k = \begin{pmatrix} 0 & f(\vec{k}) \\ f^*(\vec{k}) & 0 \end{pmatrix} \tag{2}$$

where the factor $f(\vec{k})$ is $-\sum_i t_i\ e^{i\vec{k}\cdot\vec{\delta}_i^{(0)}}$ with t_i being the hopping energy of two nearest neighbor atom. Notice that a lattice deformation changes the off-diagonal terms in the Hamiltonian which describe hopping between the two sublattices which make up the honeycomb lattice. The induced scalar potential created by strain is intensively suppressed by screening and thus we do not take it into account.

The honeycomb lattice geometry, three nearest-neighbor vectors and the lattice primitive vectors of a pristine graphene are depicted in Fig. 1. The lattice vectors are $\vec{a}_1^{(0)} = (1,\sqrt{3})\sqrt{3}a_0/2$ and $\vec{a}_2^{(0)} = (-1,\sqrt{3})\sqrt{3}a_0/2$ where $a_0 = 1.42$Å is the $C-C$ equilibrium distance. The nearest neighbor vectors are defined by

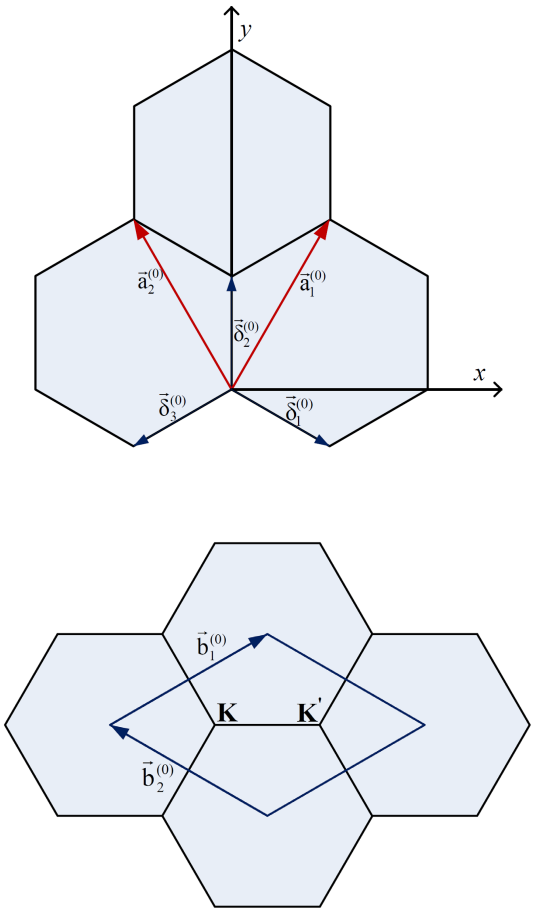

FIG. 1: (Color online) Top) Honeycomb lattice geometry incorporates three nearest-neighbor vectors and the lattice primitive vectors of pristine graphene. Bottom) The first Brillouin zone of undeformed graphene incorporates two Dirac points with high symmetry.

$$\begin{aligned} \vec{\delta}_1^{(0)} &= a_0(\frac{\sqrt{3}}{2}, -\frac{1}{2}) \\ \vec{\delta}_2^{(0)} &= a_0(0,1) \\ \vec{\delta}_3^{(0)} &= a_0(-\frac{\sqrt{3}}{2}, -\frac{1}{2}) \end{aligned} \tag{3}$$

Reciprocal lattice basic vectors are also defined by $\vec{a}_i^{(0)} \cdot \vec{b}_j^{(0)} = 2\pi\delta_{ij}$. The Brillouin zone which contains two Dirac points is shown in Fig. 1 (bottom) in which the position of $K-$point in this perfect lattice is $\vec{K} = \frac{4\pi}{3\sqrt{3}a_0}\hat{x}$. The nearest neighbor vectors in strained lattice are defined[8] by $\vec{\delta}'_{l,i} = \vec{\delta}_{l,i}^{(0)} + \sum_j \epsilon_{ij}\vec{\delta}_{l,j}^{(0)}$ and thus the modification of these distances distorts the reciprocal lattice and

it is easy to find the reciprocal vectors under strain and the results are

$$\begin{aligned}\vec{b'}_1 &= \frac{2\pi}{3\sqrt{3}d}\Big[3(1+\epsilon_{yy})-\sqrt{3}\epsilon_{xy},\sqrt{3}(1+\epsilon_{xx})-3\epsilon_{xy}\Big]\\ \vec{b'}_2 &= \frac{2\pi}{3\sqrt{3}d}\Big[-3(1+\epsilon_{yy})-\sqrt{3}\epsilon_{xy},\sqrt{3}(1+\epsilon_{xx})+3\epsilon_{xy}\Big]\ ,\end{aligned} \tag{4}$$

where $d = 1+\epsilon_{xx}+\epsilon_{yy}+O(\epsilon^2)$ and ϵ_{yx} denotes a shear strain and being zero in the uniaxial strain, respectively. The tensor for uniaxial strain along x direction is

$$\epsilon = \varepsilon\begin{pmatrix}1 & 0\\ 0 & -\nu\end{pmatrix}\ , \tag{5}$$

where $\nu = 0.165$ is Poisson's ratio. Notice that we are interested in uniform planar tension cases. Most importantly, the Dirac point which is a symmetry point, will be shifted to a new position. For homogeneous strain the position of Dirac point is defined by the condition $f(K) = 0$. After some straight forward calculations, the new position of the Dirac point is given by

$$\vec{K_D^0} = \frac{1}{2\pi}(\theta_1\vec{b}_1^{(0)}+\theta_2\vec{b}_2^{(0)}) \tag{6}$$

$$\begin{aligned}\theta_1 &= \cos^{-1}\Big(\frac{t_1^2-t_2^2-t_3^2}{2t_2t_3}\Big)\\ \theta_2 &= -\cos^{-1}\Big(\frac{t_3^2-t_2^2-t_1^2}{2t_1t_2}\Big)\end{aligned} \tag{7}$$

Notice that the reciprocal vectors of unstrained graphene appear in Eq. (6) instead of the distorted vectors,[26] and the reason of that originally comes from the tight-binding Hamiltonian and the definition of $f(k)$. In order to find the new position of the Dirac point, we only need to evaluate the hopping integrals. In fact, the change of bond-length leads to different hopping integrals among neighbors. Since the carbon atoms are out of equilibrium distance, we set[27]

$$t_i = t_0\ e^{-\frac{9.1}{t_0}(\frac{|\vec{\delta'}_i|}{a_0}-1)}\ , \tag{8}$$

where $t_0 = 3.09eV$ gives rise to $v_F = 10^6 m/s$. This definition satisfies a condition[28] in which $\partial t_i/\partial a = -6.4$ eVÅ^{-1}. The dispersion relation is thus given by $E_0(\vec{k}) = \pm|f(\vec{k})|$. For the sake of completeness, we thus expand the form factor around the K_D^0-point to obtain its low-energy expression and it results in

$$f(\vec{K_D^0}+\vec{q}) = -\sum_i t_i e^{i(\vec{K_D^0}+\vec{q})\cdot\vec{\delta}_i^{(0)}} \approx -i\sum_i t_i\vec{q}\cdot\vec{\delta}_i^{(0)}\ e^{i\vec{K_D^0}\cdot\vec{\delta}_i^{(0)}}\ . \tag{9}$$

From now on, we drop (0) index of the nearest-neighbors vectors for simplicity. Equation (9) is thus simplified as

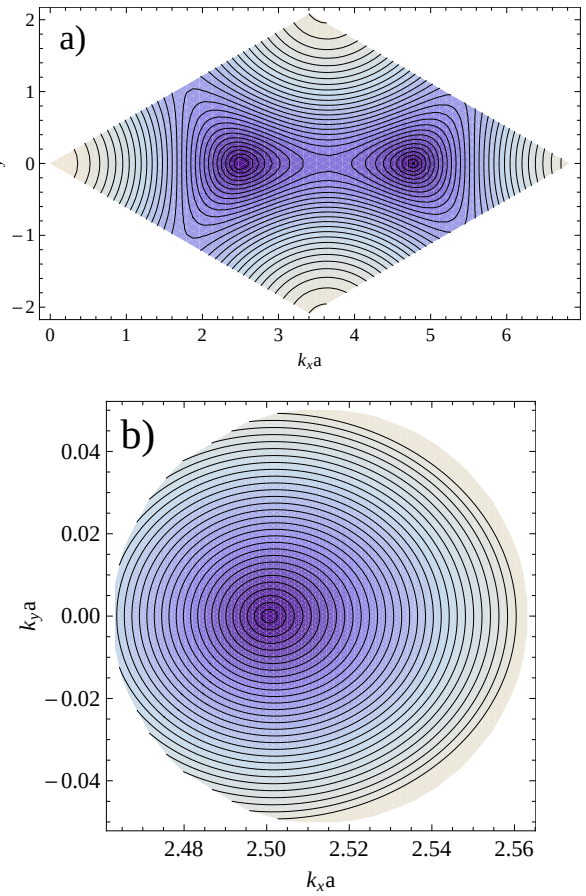

FIG. 2: (Color online) a): Contour plot of the energy dispersion for strained and interacting graphene sheet and b) a zoom of the energy dispersion around K_D-point. Notice that the center of box indicates the position of K_D^0 (shift of the Dirac point in strained graphene without the electron-electron interaction) and clearly K_D moves to the left. These results are calculated by considering $\varepsilon = 0.05$, $\alpha_{ee} = 0.5$ and $n = 10^{12}$cm^{-2}. The deviation from the linear dispersion relation associated to the trigonal warping effect is clearly shown in (a) using the full expression of $f(k)$.

$$\begin{aligned}|f(\vec{K_D^0}+\vec{q})|^2 &\approx t_1^2(\vec{q}.\vec{\delta}_1)^2+t_2^2(\vec{q}.\vec{\delta}_2)^2+t_3^2(\vec{q}.\vec{\delta}_3)^2\\ &+ (\vec{q}.\vec{\delta}_1)(\vec{q}.\vec{\delta}_3)(t_3^2-t_1^2-t_2^2)\\ &+ (\vec{q}.\vec{\delta}_1)(\vec{q}.\vec{\delta}_2)(t_2^2-t_1^2-t_3^2)\\ &+ (\vec{q}.\vec{\delta}_2)(\vec{q}.\vec{\delta}_3)(t_1^2-t_2^2-t_3^2)\end{aligned} \tag{10}$$

Therefore, the band-structure with arbitrary hopping integrals is given by

$$E_0^2 = |f(\vec{K_D}+\vec{q})|^2 = \hbar^2(v_x^2q_x^2+v_y^2q_y^2)+c^2q_xq_y\ , \tag{11}$$

where $c^2 = 3\sqrt{3}a_0^2(t_3^2-t_1^2)/2$. Since we are interested in uniaxially strained graphene along the zig-zag direction in which $t_1 = t_3$, consequently $c = 0$. In this case,

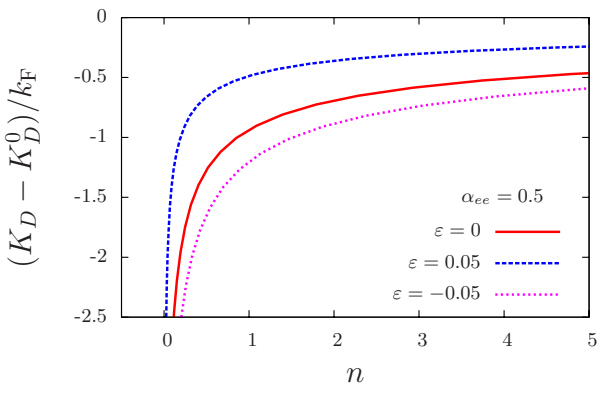

FIG. 3: (Color online) Dirac point shift in respect to the noninteracting case as a function of the electron density (in units of 10^{12} cm^{-2}) for strained and interacting graphene sheet. The Dirac point moves noticeably at the low electron density and tends to zero linearly in the high electron density.

$v_x^2 = 3a_0^2(4t_1^2 - t_2^2)/4\hbar^2$ and $v_y^2 = 9a_0^2t_2^2/4\hbar^2$. From this equation, it is obvious that the cross section of the energy dispersion in strained graphene is an elliptic shape. Accordingly, the electron velocity is direction dependent and there is an anisotropy in Fermi velocity[29]. Notice that the energy at $(q_{F_x}, 0)$ and $(0, q_{F_y})$ is equal to the Fermi energy, ϵ_F with $k_F = \sqrt{\pi n}$. Furthermore the electron density reads as $n\pi = q_{F_x}q_{F_y}$ and we thus have

$$\epsilon_F = \hbar\sqrt{v_x v_y}\sqrt{n\pi} \tag{12}$$

where $q_{F_x} = k_F\delta$, $q_{F_y} = k_F\delta^{-1}$ and $\delta = \sqrt{v_y/v_x}$.

Note that the electron density will change when we apply strain to a honeycomb lattice because the primitive cell area changes due to the strain as $\Omega' = \Omega(1 + \epsilon_{xx} + \epsilon_{yy}) = \Omega(1 + \varepsilon(1 - \nu))$ so that

$$n = \frac{n_0}{1 + \varepsilon(1 - \nu)} \tag{13}$$

where n_0 is the electron density in unstrained graphene.

B. Interacting electrons in Hartree-Fock approximation

We consider the interaction of quasiparticles by using the leading diagram approximation which is the exchange interaction. In this sense, when interactions are treated in a mean-field approximation the Hamiltonian is written as $\mathcal{H} = H_0 + H_{MF}$ where[30]

$$H_{MF} = -\frac{2}{S}\sum_{kk'}\sum_{\alpha\beta} v_{\vec{k}-\vec{k}'}\rho_{\alpha\beta}(\vec{k}')\psi^\dagger_{k\alpha}\psi_{k\beta}\ , \tag{14}$$

factor 2 stands for spin degeneracy and ρ is a density operator given by $\rho_{\alpha\beta}(\vec{k}) = (n^{(0)}_{\vec{k}+}|\psi_0^+\rangle\langle\psi_0^+| + n^{(0)}_{\vec{k}-}|\psi_0^-\rangle\langle\psi_0^-|)_{\alpha\beta}$ in which $n^{(0)}_{\vec{k}\pm}$ are noninteracting band occupation factors, v_q is the Fourier transformation of the interparticle interaction. $|\psi_0^\pm\rangle$, the eigenvectors of noninteracting Hamiltonian when the full $f(\vec{k})$ expression is considered, are given by

$$|\psi_0^\pm\rangle = \frac{1}{\sqrt{2}}\begin{pmatrix}1\\ \pm e^{-i\phi_f}\end{pmatrix} \tag{15}$$

where $\exp[i\phi_f(\vec{k})] = f(\vec{k})/|f(\vec{k})|$. After substituting Eq. 15 into the pseudospin density matrix, it can be decomposed into the charge and pseudospin-density contributions

$$\rho_{\alpha\beta}(\vec{k}) = f_+(\vec{k})\delta_{\alpha\beta} + f_-(\vec{k})\hat{n}_f.\vec{\sigma}_{\alpha\beta} \tag{16}$$

where the unit vector is $\hat{n}_f = \hat{x}\cos(\phi_f) - \hat{y}\sin(\phi_f)$ and we have introduced a short-hand notation $f_\pm = (n^{(0)}_{k+} \pm n^{(0)}_{k-})/2$.

It is easy to see that the Hamiltonian consists of a momentum-dependent pseudospin effective magnetic field which acts in the direction of momentum k. The band eigenstates in the positive and negative energy bands have their pseudospins either aligned or opposed to the direction of momentum. Therefore, the interaction mean-field Hamiltonian changes to

$$\begin{aligned}
H_{HF} &= \sum_{k\alpha\beta}\psi^\dagger_{k\alpha}\{\ \delta_{\alpha\beta}B_0(\vec{k}) + \vec{\sigma}_{\alpha\beta}.\vec{B}(\vec{k})\}\psi_{k\beta}\\
B_0(\vec{k}) &= -2\int\frac{d\vec{k}'}{(2\pi)^2}v_{\vec{k}-\vec{k}'}f_+(\vec{k}')\\
\vec{B}(\vec{k}) &= \hat{x}\Re e f(\vec{k}) - \hat{y}\Im m f(\vec{k}) - 2\int\frac{d\vec{k}'}{(2\pi)^2}v_{\vec{k}-\vec{k}'}(\hat{x}\cos(\phi_f(\vec{k}')) - \hat{y}\sin(\phi_f(\vec{k})))f_-(\vec{k}')
\end{aligned} \tag{17}$$

where the integral term of $\vec{B}(\vec{k})$ is the exchange field and the sum of the first two terms are the band-structure

pseudospin magnetic field. It should be noticed that Eq. (17) is our main theoretical result. At zero temperature and for an n-doped graphene layer, $f_+(\vec{k}) = \frac{1}{2}\theta(\epsilon_F - \epsilon_{\vec{k}}) + \frac{1}{2}$ and $f_-(\vec{k}) = -\frac{1}{2}\theta(\epsilon_{\vec{k}} - \epsilon_F)$ where ϵ_F and $\epsilon_{\vec{k}}$ are the Fermi energy and the noninteracting energy dispersion, respectively. To account partially for screening and to avoid the well-known Fermi velocity artifact of mean-field theory in systems with long-range interactions, we have used an interaction potential including Thomas-Fermi screening

$$v_{k-k'} = \frac{2\pi e^2}{\bar{\epsilon}(q_{TF} + |\vec{k} - \vec{k'}|)} \ , \tag{18}$$

where $q_{TF} = \alpha_{ee} k_F$ is the Thomas-Fermi screening vector and $\alpha_{ee} = e^2/(\bar{\epsilon}\hbar v_F)$ is the graphene coupling constant, which is density independent. $\bar{\epsilon}$ is an average dielectric constant of the surrounding medium.

Notice that in our calculations, all integrals in the phase space are taken over the first Brillouin zone that is, a primitive unit cell of the reciprocal lattice (see Fig. 1 (bottom). For the sake of simplicity, it is convenient to work in a frame (k_1, k_2) where k_1 and k_2 are along $\vec{b'}_1$ and $-\vec{b'}_2$, respectively. Therefore, it is accomplished by changing $k_x = b'_{1,x}(k_1 + k_2)/|\vec{b'}_1|$ and $k_y = b'_{1,y}(k_1 - k_2)/|\vec{b'}_1|$ where the Jacobian is

$$J = 2\frac{b'_{1,x} b'_{1,y}}{|\vec{b'}_1|^2} = 6\sqrt{3}\frac{(1-\nu\varepsilon)(1+\varepsilon)}{9(1-\nu\varepsilon)^2 + 3(1+\varepsilon)^2} \tag{19}$$

The real and imaginary part of $f(k)$ are given by $\Re e f(\vec{k}) = -\sum_l t_l \cos(\vec{k}\cdot\vec{\delta}_l)$ and $\Im m f(\vec{k}) = -\sum_l t_l \sin(\vec{k}\cdot\vec{\delta}_l)$, respectively. After having all ingredients, we are able to write the energy dispersion in HF approximation

$$E_\pm(\vec{k}) = B_0(k) \pm \sqrt{B_x(\vec{k})^2 + B_y(\vec{k})^2} \ . \tag{20}$$

Once $B_0(k)$ and $\vec{B}(\vec{k})$ are obtained, the ground state quantities can be calculated. Due to the exchange interaction, the Dirac points are shifted and a new Dirac point, K_D is found by searching the zeroth of Eq. (20).

C. Anisotropy renormalized Fermi velocity and charge compressibility

The effective Fermi velocity is an important concept in Landau's Fermi liquid theory since it provides a direct measure of the many-body interactions in the electron system. The low-energy electronic excitations in graphene are described by a massless Dirac Hamiltonian that is able to explain many transport properties. The Fermi velocity is the only parameter that appears in the model Hamiltonian and it plays the same role as the effective mass[31] in the standard Landau's Fermi liquid theory. The renormalized Fermi velocity can be calculated

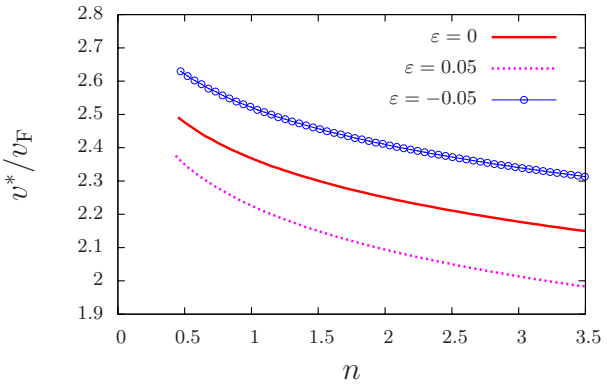

FIG. 4: (Color online) Strain dependence of the renormalized velocity at $(q_{F_x}, 0)$ point, scaled by that of a noninteracting velocity as a function of the electron density (in units of 10^{12} cm^{-2}) for different strain values and $\alpha_{ee} = 0.9$. Since the dispersion relation has an elliptic shape, the Fermi velocity has also an anisotropic form. For the positive strain values, stretching the sample, the renormalized Fermi velocity at $(q_{F_x}, 0)$ point suppresses however, the renormalized Fermi velocity enhances by compressing the sheet. Importantly, the strain dependence of the Fermi velocity behaves differently as the sign of the strain is changed.

when the ground state energy dispersion as a function of $\vec{k}$ is obtained. The renormalized Fermi velocity can be expressed[32] in terms of the wavevector derivative of the charge carrier dispersion relation evaluated at the Fermi surface

$$\vec{v^*} = \frac{1}{\hbar}\vec{\nabla} E(\vec{k})|_{\vec{k}=\vec{K}_D+\vec{q}_F} \ , \tag{21}$$

and therefore, the Fermi velocity component along ith-direction is given by

$$\hbar v_i^* = \frac{\partial B_0(k)}{\partial k_i} + \frac{B_x(k)\frac{\partial B_x(k)}{\partial k_i} + B_y(k)\frac{\partial B_y(k)}{\partial k_i}}{\sqrt{B_x(k)^2 + B_y(k)^2}}|_{\vec{k}=\vec{K}_D+\vec{q}_F} \tag{22}$$

Once the ground state is obtained the compressibility, κ can be easily calculated from

$$\frac{1}{n^2\kappa} = \frac{\partial \mu}{\partial n} \tag{23}$$

where μ is the chemical potential of quasiparticles and incorporates the kinetic energy and the first order exchange interaction in the presence of the uniaxial strain. Therefore, it is easy to get the following expression.

$$\frac{\partial \mu}{\partial n} = \frac{\partial k_F}{\partial n}\frac{\partial \mu}{\partial k_F} \ , \tag{24}$$

in which $\partial k_F/\partial n = k_F/(2n)$. Notice that the compressibility of the noninteracting system at low- energy is

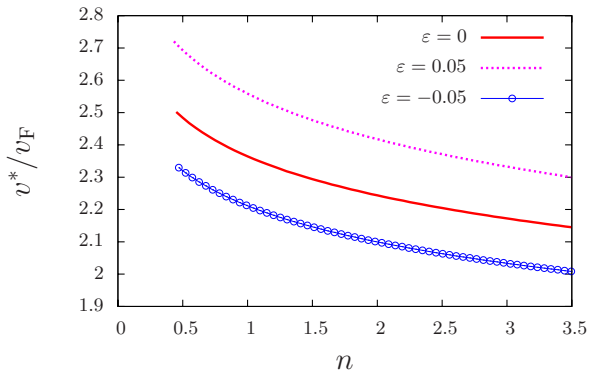

FIG. 5: (Color online) Strain dependence of the renormalized velocity at $(0, q_{F_y})$ point, scaled by that of a noninteracting velocity as a function of the electron density (in units of 10^{12} cm^{-2}) for different strain values and $\alpha_{ee} = 0.9$. For the positive strain values, stretching the sample, the renormalized Fermi velocity at $(0, q_{F_y})$ point is enhanced however, the renormalized Fermi velocity is suppressed by compressing the sheet. The strain dependence of the Fermi velocity behaves differently with those results obtained at $(q_{F_x}, 0)$.

given by $\kappa_0 = 2/(n\hbar\sqrt{v_x v_y}\sqrt{\pi n})$. The expression reduces to the well-known expression of the noninteracting compressibility by setting $v_x = v_y$.

III. NUMERICAL RESULTS

In this section, we present our calculations for the ground-state properties of graphene in the presence of uniaxial strain which we model as mentioned above. The shift of Dirac points, the anisotropy of the Fermi velocity renormalization and inverse compressibility $1/(n^2\kappa)$ are calculated by using the theoretical models and we compared the latter with the recent experimental measurements. In all numerical calculations presented here, we take into account the full Brillouin zone by using the expression of $f(\vec{k})$. In this case, accurate calculations require dense $k-$ point sampling near the Dirac point and thus we use a dense adaptive sampling model the same as used in Ref. [33]. We have also dropped the constant 1/2 contribution from the integrand of $B_0(\vec{k})$ and the reason is that the latter term produces a constant energy contribution.

As we have discussed in the previous section, the Dirac point moves to a new position by taking into account the full $f(k)$ in strained and interacting graphene. The contour plot of the massless Dirac excitation energy is shown in Fig. 2 for $\alpha_{ee} = 0.5$. Notice that the center of the Fig. 2(b) indicates the position of K_D^0 (the Dirac shift of strained graphene without the electron-electron interaction) and clearly K_D moves to the left. It is also clear from the figure that the Dirac points, defined by

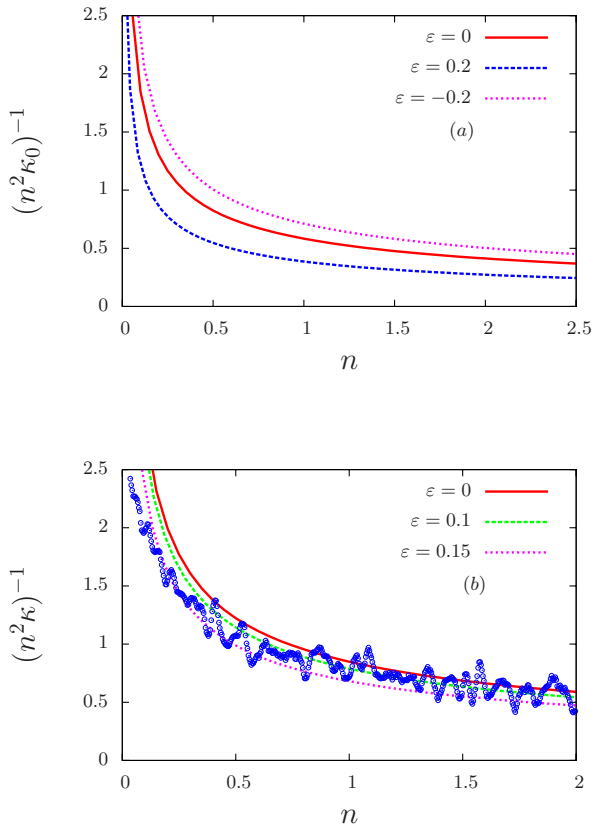

FIG. 6: (Color online) The inverse compressibility $[n^2\kappa]^{-1} = \partial\mu/\partial n$ (in units of meV 10^{-10}cm^2) as a function of the electron density (in units of 10^{12} cm^{-2}) for different strain values for (a) a noninteracting and (b) an interacting massless Dirac electron system in graphene sheets. The symbols are the experimental data by Martin *et al.*[35]. The strain dependence of the charge compressibility behaves differently as the sign of the uniaxial strain is changed. The coupling constant is $\alpha_{ee} = 0.26$.

$E_+(\vec{K}_D) = E_-(\vec{K}_D)$, are not exactly on the K_D^0 and $K_D^{\prime 0}$ points. It is easy to show that B_y vanishes along x direction for the uniaxial strain. Since $B_0(K_D)$ does not vanish, we might define an energy shift so that to get vanishing dispersion relation at the Dirac point. Therefore, the excitation energy is redefined as $\mathcal{E}(\vec{k}) = E(\vec{k}) - E(\vec{K}_D)$. A deviation from the linear dispersion relation associated to the trigonal warping effect is clearly shown in Fig. 2(a) using the full expression of $f(\vec{k})$.

It is noticed that in a noninteracting graphene system, the Dirac point is given by Eq. (6) and it differs with $K = 4\pi/(3\sqrt{3}a_0)$ when the lattice is unperturbed. Due to the charge-charge interaction, the Dirac point changes and the shift is found by searching the zeroth of Eq. (20). The Dirac shift, $K_D - K_D^0$ scaled by k_F, as a function of the electron density (in units of 10^{12} cm^{-2}) is depicted in Fig. 3. The shift is noticeable at the low electron density

region and tends to zero linearly in the high densities. It is worthwhile mentioning that the Dirac shift value is enhanced when a graphene is compressed however, it is suppressed when a graphene sheet is stretched. In addition, the shift disappears[30] in the linear limit of $f(\vec{k})$ expression.

Our results for the strain dependence of the Dirac electron velocity, $v^\star/v_{\rm F}$, at $(q_{{\rm F}_x},0)$ point as a function of the electron density n are demonstrated in Fig. 4. Since the dispersion relation has an elliptic shape, the Fermi velocity has an anisotropic form. The numerical results are shown for different strain values, ε and for the graphene coupling constant, $\alpha_{ee}=0.9$. For the positive strain values, by stretching the sample, the renormalized Fermi velocity at $(q_{{\rm F}_x},0)$ point suppresses, however the renormalized Fermi velocity enhances by compressing the sheet. These behaviors are based on the effective hopping terms in the presence of the strain. Besides, the Fermi velocity decreases by increasing the electron density due to the exchange interactions between electrons near the Fermi surface. The strain dependence of the Dirac electron velocity at $(0,q_{{\rm F}_y})$ point, on the other hand, behaves differently with those results obtained at $(q_{{\rm F}_x},0)$ point and our numerical results are shown in Fig. 5. As the uniaxial strain increases along the dirction of graphene deformation, the Fermi velocity in this direction decreases quickly, whereas the Fermi velocity perpendicular to it increases.

Recently, the uniaxial deformation of graphene on the unidirectionally modulated SiC steps shaped substrate is studied by using angular resolved photoemission spectroscopy[34]. A reduction of the Fermi velocity along the direction of graphene deformation, v_x was observed, while in another direction the changes were not significant. Our numerical results on the Fermi velocity along the direction of graphene deformation are in good agreement with the recent observations. The reason for the insensitivity of the Fermi velocity perpendicular to the graphene deformation, v_y is probably due to the fact that the sample is shaped as a supperlattice along the direction of deformation. The sample can be roughly realized as a combination of a pristine supperlattice graphene together with a uniaxial strained ribbon. For the pristine supperlattice, v_y decreases and v_x remains unchanged. On the other hand, we show that v_y increases when graphene is stretched and therefore there should be a cancellation between two contributions and it leads to insensitivity of the Fermi velocity perpendicular to the direction of graphene deformation in agreement with the experimental measurements.

The local compressibility of graphene, on the other hand, has been measured [35] using a scannable single electron transistor. From the theoretical point of view, the compressibility was also studied by different groups at zero temperature[15,19,36] and also at finite temperature[37]. In order to calculate the charge compressibility in the presence of strain, we do need to calculate the derivative of the total energy as a function of the electron density. It should be noted that $\partial B_0(\vec{k})/\partial k_{\rm F}$ and $\partial \vec{B}(\vec{k})/\partial k_{\rm F}$ change slightly by changing $\phi=\tan^{-1}(k_y/k_x)$ which is a consequence of the elliptic shape of the Fermi surface and the ϕ dependence tends to zero for small ε values. Our numerical compressibility is obtained by taking an average over ϕ and the results are shown in Fig. 6. The strain dependence of the compressibility for a noninteracting system is also demonstrated in Fig. 6(a). For the noninteracting case, it is easy to find that $\sqrt{v_x v_y}\propto v_{\rm F}(1-9.1(1-\nu)\varepsilon/(8t_0))$ and thus for $\varepsilon>0$ it gives rise to a reduction of the inverse of the compressibility. Importantly, the charge compressibility decreases (increases) by compressing (stretching) a graphene sheet. Also the asymmetric response to the positive and negative strain is evident in the charge compressibility as is evident in the renormalized Fermi velocity.

In Fig. 6(b) we compare our theoretical predictions for the inverse compressibility of doped graphene with the experimental results of Martin *et al.*[35] as a function of the electron density in units of 10^{12} cm^{-2}. Martin *et al.*[35] fitted the experimental inverse compressibility, $(n^2\kappa)^{-1}$ to the kinetic term using a single parameter Fermi velocity which is larger than the bare Fermi velocity. Note that the kinetic term in graphene has the same density dependence as the leading exchange and correlations terms[19].

As it is clear in Fig. 6(b) the inverse compressibility of an interacting system is higher than the experimental value. By increasing the uniaxial strain effects, i.e., increasing the constant strength, ε our theoretical results move down. Therefore, including the exchange and strain effects in our theory, gives results very close to experimental data.

IV. CONCLUSION

We have studied the ground state properties of a graphene sheet within the Hartree-Fock theory incorporating the uniaxial strain in the system. We have shown that the quasiparticle properties could be strongly strain dependent and substantially different than the usual pristine graphene sheet. The Dirac points move due to the strain and the anisotropy of Fermi velocity renormalization is obtained. The Dirac electron Fermi velocity is highly dependent on the sign of strain (stretching or compressing) even if the strain is negligibly small. The renormalized electron velocity along the direction of graphene deformation decreases with stretching however, it increases by compressing the graphene sample. The Fermi velocity along a direction perpendicular to graphene deformation behaves in a different way. We find the reduction of Fermi velocity along the direction of graphene deformation to be in good agreement with the recent experimental observation.

Our calculations of inverse compressibility compared with recent experimental results of Martin *et al.*[35] demonstrate the important influence of strain on the thermodynamic quantities in a graphene sample.

We remark that in a very small density region, the system is highly inhomogeneous and the effect of strain might be very essential. A model going beyond the Hartree-Fock approximation is necessary to account for increasing correlation effects at low density.

Acknowledgments

We thank S. Abedinpour for useful discussions. This work was supported by IPM.

* Electronic address: asgari@ipm.ir

[1] K.S. Novoselov, A.K. Geim, S.V. Morozov, D. Jiang, Y. Zhang, S.V. Dubonos, I.V. Grigorieva, A.A. Firsov, Science **306**, 666 (2004); A. K. Geim and K. S. Novoselov, Nature Mater. **6**, 183 (2007); A. H. Castro Neto, F. Guinea, N. M. R. Peres, K. S. Novoselov, and A. K. Geim, Rev. Mod. Phys. **81**, 109 (2009) .

[2] Valeri N. Kotov, Bruno Uchoa, Vitor M. Pereira, A. H. Castro Neto, F. Guinea, Rev. Mod. Phys. **84**, 1067 (2012) .

[3] A. Bostwick, F. Speck, T . Seyller, K. Horn, M. Polini, R. Asgari, A.H. MacDonald, and E. Rotenberg, Science **328**, 999 (2010) .

[4] P. Avouris, Z. Chen, and V. Perebeinos, Nature Nanotech. **2**, 605 (2007); A. K. Geim, Science **324**, 1530 (2009). F. Bonaccorso, Z. Sun, T. Hasan, and A. C. Ferrari, Nat. Photon. **4**, 611 (2010) .

[5] Seon-Myeong Choi, Seung-Hoon Jhi and Young-Woo Son Phys. Rev. B **81**, 081407(R),(2010); Marcel Mohr, Konstantinos Papagelis, Janina Maultzsch and Christian Thomsen Phys. Rev. B **80**, 205410 (2009); F. M. D. Pellegrino, G. G. N. Angilella and R. Pucci1,*ibid* **81**, 035411 (2010) .

[6] Vitor M. Pereira and A. H. Castro Neto, and N. M. R. Peres, Phys. Rev. B ,**80**, 045401 (2009)

[7] C. Lee, X. Wei, J. W. Kysar, J. Hone, Science **321**, 385 (2008); W. Bao, F. Miao, Z. Chen, H. Zhang, W. Jang, C. Darmes, C. N. Lau, Nat. Nanotechnology **4**, 562 (2009) .

[8] H. Suzuura and T. Ando, Phys. Rev. B **65**, 235412 (2002) .

[9] J. L. Manès, Phys. Rev. B **76**, 045430 (2007) .

[10] M. A. H. Vozmediano, M. I. Katsnelson, F. Guinea, Phys. Reports **496**, 109 (2010); F. Guinea, Solid State Communi. **152**, 1437 (2012) .

[11] N. Levy, S. A. Burke, K. L. Meaker, M. Panlasigui, A. Zettl1, F. Guinea, A. H. Castro Neto and M. F. Crommie, Science **329** , 554 (2010) .

[12] N. Abdedpour, R. Asgari and F. Guinea, Phys. Rev. B **84**, 115437 (2011) .

[13] F. Guinea, M. I. Katsnelson, A. K. Geim, Nat. Phys. **6**, 30 (2010); K. Gomes, et al Nature (London) **483**,306 (2012) .

[14] Zhen Hua Ni, Ting Yu, Yun Hao Lu, Ying Ying Wang, Yuan Ping Feng, and Ze Xiang Shen, ACS Nano **2**, 2301 (2008); K. S. Kim, Y. Zhao, H. Jang, S. Y. Lee, J. M. Kim, K. S. Kim, J. H. Ahn, P. Kim, J. Choi, and B. H. Hong, Nature (London) **457**, 706 (2009); T. M. G. Mohiuddin, A. Lombardo, R. R. Nair, A. Bonetti, G. Savini, R. Jalil, N. Bonini, D. M. Basko, C. Galiotis, N. Marzari, K. S. Novoselov, A. K. Geim, and A. C. Ferrari, Phys. Rev. B **79**, 205433 (2009); M. Y. Huang, H. G. Yan, C. Y. Chen, D. H. Song, T. F. Heinz and J. Hone, Proc. Natl. Acad. Sci. U.S.A. **106**, 7304 (2009); M. L. Teague, A. P. Lai, J. Velasco, C. R. Hughes, A. D. Beyer, M. W. Bockrath, C. N. Lau, N.-C. Yeh, Nano Lett. **9**, 2542 (2009); N. Ferralis, R. Maboudian, and C. Carraro, Phys. Rev. Lett. **101**, 156801 (2008) .

[15] Y. Barlas, T. Pereg-Barnea, M. Polini, R. Asgari and A. H. MacDonald, Phys. Rev. Lett. **98**, 236601 (2007) .

[16] M. Polini, R. Asgari, Y. Barlas, T. Pereg-Barnea and A.H. MacDonald, Solid State Commun. **143**, 58 (2007) .

[17] A. Qauimzadeh and R. Asgari, Phys. Rev. B **79**, 075414 (2009) .

[18] A. Qauimzadeh, Kh. Jahanbani and Reza Asgari, Phys. Rev. B **85**, 235428 (2012) .

[19] R. Asgari, M, M. Vazifeh, M. R. Ramezanali, E. Davoudi and B. Tanatat, Phys. Rev. B **77**, 125432 (2008) .

[20] D. C. Elias, R. V. Gorbachev, A. S. Mayorov, S. V. Morozov, A. A. Zhukov, P. Blake, L. A. Ponomarenko, I. V. Grigorieva, K. S. Novoselov, F. Guinea, A. K. Geim, Nat. Phys. **7**, 701 (2011) .

[21] A. Luican, G. Li, and E. Y. Andrei, Phys. Rev. B **83**, 041405 (2011); D. A. Siegel, C. Park, C. Hwang, J. Deslippe, A. V. Fedorov, S. G. Louie, and A. Lanzara, Proc. Natl. Acad. Sci. USA. **108**, 11365 (2011) .

[22] Seon-Myeong Choi, Seung-Hoon Jhi, and Young-Woo Son, Phys. Rev. B **81**, 081407 (2010) .

[23] Anand Sharma and Valeri N. Kotov, A. H. Castro Neto, arXiv:1206.5427 (2012) .

[24] V. K. Dugaev and M. I. Katsnelson, arXiv:1206.4526 (2012) .

[25] K. Sasaki, Y. Kawazoe and R. Saito, Prog. Theor. Phys. 113, 463480 (2005); S. V. Morozov et al., Phys. Rev. Lett. **97**, 016801 (2006) .

[26] Yasumasa Hasegawa, Rikio Konno, Hiroki Nakano and Mahito Kohmoto, Phys. Rev. B **74**, 033413 (2006) .

[27] D. A. Papaconstantopoulos, M. J. Mehl, S. C. Erwin, and M. R. Pederson*in Tight-Binding Approach to Computational Materials Science*, edited by P. Turchi, A. Gonis, and L. Colombo Materials Research Society, Pittsburgh, (1998) .

[28] A. H. Castro Neto and F. Guinea, Phys. Rev. B **75**,045404 (2007) .

[29] F. M. D. Pellegrino, G. G. N. Angilella and R. Pucci, Phys. Rev. B **84**, 195404 (2011) .

[30] G. Borghi , M. Polini , R. Asgari , A.H. MacDonaldd, Solid State Communications ,**149**, 1117 (2009) .

[31] R. Asgari and B. Tanatar, Phys. Rev. B **74**, 075301 (2006) .

[32] G.F. Giuliani and G. Vignale, *Quantum Theory of the Electron Liquid* (Cambridge University Press, Cambridge, 2005) .

[33] Jeil Jung and Allan H. MacDonald, Phys. Rev. B **84**, 085446 (2011) .

[34] Kan Nakatsuji, Tsuguo Yoshimura, and Fumio Komori, Kouhei Morita and Satoru Tanaka, Phys. Rev. B **85**, 195416 (2012) .

[35] J. Martin, N. Akerman, G. Ulbricht, T. Lohmann, J. H. Smet, K. von Klitzing, and A. Yacoby, Nat. Physics, **4**, 144 (2008) .

[36] N.M.R. Peres, F. Guinea, and A.H. Castro Neto, Phys. Rev. B **72**, 174406 (2005); E.H. Hwang, B.Y.-K. Hu, and

S. Das Sarma, Phys. Rev. Lett. **99**, 226801 (2007); D.E. Sheehy and J. Schmalian, *ibid* **99**, 226803 (2007) .

[37] M.R. Ramezanali, M.M. Vazifeh, Reza Asgari, Marco Polini, A.H. MacDonald, J. Phys. A : Math. Theor. **42**, 214015 (2009); A. Faridi, M. Pashangpour, R. Asgari, Phys. Rev. B **85**, 045410 (2012) .